Uncertainties in the Swift hardening law parameters and their influence on the flow stress and the hole expansion behavior of dual-phase (DP600) steel specimens

Article *in* Journal of Materials Engineering and Performance · December 2022

4 authors:

Kali Prasad
Indian Institute of Technology Madras

Deepak Kumar
Indian Institute of Technology Madras

Hariharan Krishnaswamy
Indian Institute of Technology Madras

Dilip Kumar Banerjee
National Institute of Science & Technology

Uncertainties in the Swift hardening law parameters and their influence on the flow stress and the hole expansion behavior of dual-phase (DP600) steel specimens

Kali Prasad[1*], Deepak Kumar[2], Hariharan Krishnaswamy[1] and Dilip K. Banerjee[3]

[1*]Department of Mechanical Engineering, Indian Institute of Technology Madras, Chennai, 600036, Tamil Nadu, India.
[2]Department of Applied Mechanics, Indian Institute of Technology Madras, Chennai, 600036, Tamil Nadu, India.
[3]Material Measurement Laboratory, National Institute of Standards and Technology (NIST), Gaithersburg, Maryland, 20899, USA.

*Corresponding author(s). E-mail(s): kali.iitm@gmail.com, kprasad@alumni.iitm.ac.in;
Contributing authors: dksharma280591@gmail.com; hariharan@iitm.ac.in; dilip.banerjee@nist.gov;

Abstract

Swift hardening law is one of the widely used phenomenological model to describe the stress-strain behavior in sheet metal forming simulations. In the present study, a statistical approach was used to investigate the effect of the variation in material model parameters on estimated values of the stress-strain data obtained using Swift hardening law. This estimation employed values of the Swift hardening law parameters as reported in the literature and those from three uniaxial tensile tests conducted in this study. Uncertainties in the flow stress were estimated using Monte Carlo (MC) simulations. A detailed sensitivity analysis was performed to

*Current affiliation: Graduate Institute of Ferrous Technology, Pohang University of Science and Technology (POSTECH), Pohang, 37673, Republic of Korea

determine the most sensitive parameter influencing the flow stress estimation. It was found that the sensitivity coefficients of the Swift hardening parameters are dependent on the true plastic strain. At lower plastic strains $\boldsymbol{\epsilon_0}$ was found to be most sensitive parameter whereas at larger pre-strains $\boldsymbol{K}$ was observed to be the critical parameter affecting the flow stress estimation. Further, computed hardening curves were used to simulate the deformation in hole expansion tests (HET) of dual phase steel (DP600) steel specimens using an explicit finite element analysis (FEA) technique. The effects of the material property variation on the thinning rate of the sheet with punch displacement were estimated with a mean ($\boldsymbol{\mu}$) and standard deviations ($\boldsymbol{\sigma}$) for determining ($\pm$ 1$\boldsymbol{\sigma}$, $\pm$ 2$\boldsymbol{\sigma}$) statistical limits. FEA predictions were compared with measured data obtained from HET conducted using specimens with holes fabricated with both drilling and boring processes. A reasonable agreement was achieved. Furthermore, the experimental values of the final sheet thicknesses were found to lie within the statistical limits using finite element simulations.

Keywords: Uncertainty quantification, Sheet metal forming, Monte Carlo method, Dual-phase steel, Finite element analysis, Hole expansion test

1 Introduction

The demand for accurate numerical predictions of forming automotive components is continuously increasing. Often, the design of these components is performed using finite element (FE) simulations. These forming simulations are conducted at large strains typically reached in forming operations. Stress-strain data are usually developed by conducting uniaxial tensile tests that result in reliable data up to the limit of uniform elongation. Therefore, true stress vs. true strain data must be extrapolated beyond this point to be used in a FE material model. Typically, the experimental true stress - true strain response is extrapolated to large plastic strains using suitable phenomenological strain hardening models to describe the post-necking deformation behavior [1, 2]. The parameters of strain hardening models are estimated using fitting the experimental true stress-strain data obtained from tensile tests. The accuracy of numerical simulations largely depends on the accuracy of identified hardening parameters. Generally, there are uncertainties associated with the estimated hardening parameters. These can be attributed to (a) inherent strain measurement uncertainty associated with measuring devices such as extensometers, strain gauges, digital image correlation (DIC) [3–5] etc., (b) statistical randomness, (c) metallurgical factors like grain size [6], chemical composition, coil-to-coil variation during sheet rolling [7], experimental limitations associated with measurement tools [6, 8], etc. Scatter in material properties, and boundary conditions that rely on experimental measurements are a significant source of errors affecting the FE simulations' accuracy. In the scientific measurement system, uncertainty analysis is an essential component, as it assesses

the effect of the variability in input variables on the output and the system response. In general, uncertainties associated with a measurement system can be classified into two broad categories, (i) Aleatoric (random) (ii) Epistemic (systematic). Aleatoric uncertainties [9] are associated with the inherent randomness within the measuring system and cannot be minimized or removed. Epistemic uncertainties are knowledge-based uncertainties that robust models and algorithms can reduce. Thus, the proper applicability of numerical simulation results can be ascertained by knowing both the aleatoric and epistemic uncertainty.

Numerous studies have been performed by various researchers to understand the uncertainty associated with the deformation behavior of materials subjected to mechanical loading [10–13]. For instance, while estimating the service life of components subjected to fatigue loading or while evaluating the formability of sheet metal using traditional formability tests like forming limit diagram (FLD), limiting dome height (LDH), several factors such as testing environment, loading cycle, geometric parameters, etc. [12–14] were found to play a critical role. De Souza and Rolfe et al. [15] reported the effect of deformation conditions like blank holding pressure (BHP) and friction conditions on the springback characteristics in dual-phase steels. In this work, the authors showed that the variations in mechanical behavior had an appreciable influence on springback. Similar work was performed by the same authors, in which a probabilistic analytical model was proposed to account for the variations in input parameters for predicting springback [16]. Karthik et al. [17] systematically studied the effect of material property variation on formability in different grades of ferritic stainless steels obtained from different coils. Standard uniaxial tensile tests and LDH tests were performed in different coil specimens, and it was concluded that there were significant variations in the formability of these specimens. Formability variations in the rolling direction were always higher compared to that in the transverse direction. An analysis of the scatter in published data reported by researchers as mentioned above demonstrates that it is due to a combined effect of geometrical inhomogeneity, change in strain path [18, 19], friction condition [20, 21] and material effect [10, 12, 22]. Fundamental material behavior has a very important role in the scatter associated with characteristics of these plastic deformation processes. The component of scatter associated with material property has not been investigated so far. MC simulation is a stochastic analysis that has been widely used to model the scatter in deformation behavior in metal forming [13, 23]. In spite of several stochastic studies discussed above, there has not been a systematic investigation of the uncertainty associated with the hardening law parameters and their implications in sheet metal forming simulations. The close resemblance of hole expansion deformation process with the uniaxial tensile test in terms of the evolving stress state is likely to give important insights on the deformation process.

In the present work, we have investigated the effect of variability in material model parameters, which forms a very critical part of the analysis. Despite the

widespread use of the Swift hardening law in sheet metal forming applications [24–27], stochastic-based analysis considering the scatter in material properties has not been conducted. Therefore, the objective of the present study is to systematically investigate the effect of cumulative uncertainty associated with material property scatter and errors in estimating the parameters of the Swift hardening model. The Swift hardening law, is widely used for performing sheet metal forming simulations [24–27]. Dual-phase steel (DP 600) is chosen in this study because it finds widespread use in the automotive sector. Further, statistical analysis was performed to understand the effect of material property scatter and uncertainty associated while obtaining the coefficients of hardening parameters from experimental data. Furthermore, the influence of uncertainty in hardening parameters was studied using a practical sheet metal forming simulation. The hole expansion test (HET) is a standard sheet metal test to evaluate the stretch-flangeability of the material [28–31]. This test determines the ability of the sheet metal to resist edge deformation. Various researchers have studied the hole expansion deformation process and showed that the hole edge deforms in an uniaxial stress state [29–32]. Hence, the scatter in tensile properties will directly affect the accuracy of the test results. Therefore, the hole expansion test was chosen as an application example in the present work. Finite Element simulation of hole expansion test was performed to understand the deformation process. The influence of scatter in material properties on sheet thinning and equivalent fracture strains were estimated for the mean (μ) with ($\pm 1\sigma$) and ($\pm 2\sigma$) standard deviation (σ) limits representing the confidence intervals of 68% and 95% respectively. The novelty of the present work is that it provides shop floor engineers a tool to identify the scatter and uncertainties in hardening law parameters when same type of materials from different metallurgical heats are used in routine forming operations. Additionally, this study provides a systematic approach to identify the most important hardening parameters that influence the material deformation behavior in the strain range of interest. This study can be easily extended to more complicated hardening laws, when the appropriate probability distributions of the hardening parameters can be accurately identified by systematically analyzing stress-strain data from tests and/or from a literature review.

2 Statistical analysis of material data

2.1 Sample data

In this study, the variation of the material parameters of the Swift hardening law for DP600 steel was chosen:

$$\bar{\sigma}_Y = K(\epsilon_o + \epsilon_p)^n \tag{1}$$

where, $\bar{\sigma}_Y$ is flow stress, K, ϵ_0, and n are material parameters.
The values of these parameters are collected from the literature and summarized in Table 2. It can be seen from the Table 2 that the parameters vary

significantly. The variations in the parameters represent scatter in the material properties [1]. Additionally, uniaxial tensile tests were conducted to obtain the parameters by fitting the experimental stress-strain data. DP600 steel with nominal chemical composition (in wt.%: C-0.08, Si-0.13, Mn-0.94, Cr-0.57, Ni-0.017, Al-0.03, S-0.005, P-0.039, Fe-balance) was selected. Tensile tests were performed in a Zwick/Roell Z100 100 kN [2] universal tensile testing machine (Fig.1). The tensile test was conducted at a nominal strain rate of 1 e^{-3} s^{-1}. Tensile test specimens were prepared according to the ASTM E8 standard [33] sub-size specimen along the sheet's rolling direction (RD), Transverse direction (TD) and 45° to RD. Strain measurements were recorded using a non-contact type video extensometer. The Lankford coefficients were estimated from the experimental data and are presented in the Table 1. The experiment was repeated three times to assess statistical uncertainty. The parameters K, ϵ_0, and n were obtained by curve fitting the experimental data.

[1] The variations in the material properties can be attributed to variations in chemical composition, microstructure, measurement errors, etc.

[2] Certain commercial equipment, instruments, software, or materials are identified to adequately describe a procedure or concept. Such identification is not intended to imply recommendation, endorsement, or implication by NIST that the equipment, instruments, software, or materials identified are necessarily the best available for the purpose.

Table 1: Coefficients of lankford parameters

r_0	r_{45}	r_{90}	$\overline{r}$
0.742	1.01	0.782	0.866

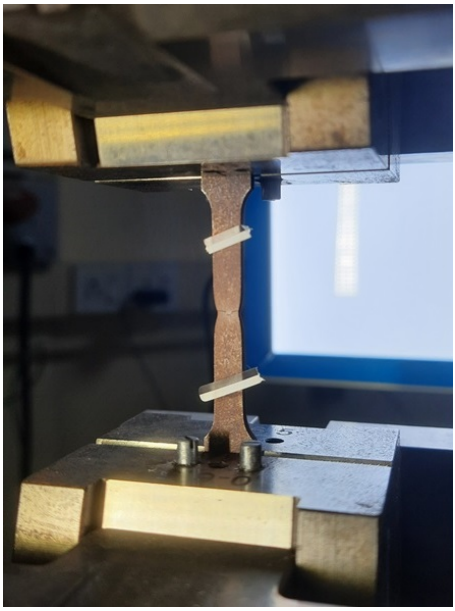

Fig. 1: Image showing the tensile specimen being tested in a universal testing machine.

Table 2: Parameters for the Swift hardening law for DP600 steel.

S.no.	K (MPa)	ϵ_0	n	Reference
1	1042.3	0.0224	0.231	[34]
2	1017	0.0032	0.182	[26]
3	1387	0.03	0.299	[35]
4	1019	0.0024	0.178	[24]
5	1078.91	0.0025	0.198	[36]
6	904	0.0175	0.182	[37]
7	970	0.0078	0.145	[38]
8	1080	0.001	0.152	[39]
9	1067.2	0.002	0.192	[40]
10	1140	0.005	0.2	[41]
11	1000	0.005	0.218	[42]
12	1201.75	0.0036	0.214	[43]
13	1101	0.002	0.22	[44]
14	1045.77	0.003	0.19	[45]
15	1140	0.005	0.2	[46]
16	983	0.0023	0.19	[47]
17	1140	0.001	0.203	[48]
18	1056	0.002	0.203	[49]
19	1063.9	0.0023	0.153	[50]
20	1054.2	0.0016	0.201	[51]
21	1243	0.003	0.216	[52]
22	1004	0.002	0.16	[53]
23	1044	0.0045	0.16	[54]
24	1177	0.0003	0.177	[55]
25	1140	0.005	0.2	[56]
26	1170	0.004	0.21	[18]
27	1207.8	0.0065	0.222	[25]
28	790.2	0.0008	0.132	[57]
29	1043	0.0005	0.184	[58]
30	945.5	0.002	0.22	[59]
31	1093	0.005	0.187	[27]
32	1100	0.02	0.2	[60]
33	1016.96	0.0051	0.173	[61]
34	983	0.0023	0.19	[62]
35	988	0.005	0.182	[63]
36	1077.3	0.0042	0.202	[64]
37	1261	0.004	0.16	[65]
38	1093	0.0016	0.187	[66]
39	1093	0.0016	0.187	[67]
40	1040 ± 3	0.005 ± 0.00055	0.166 ± 0.003	Present work

2.2 MC method for computing uncertainty

MC simulation is one of the most widely used probabilistic methods used to estimate uncertainty in the response variable. This method is based on randomly generated input process variables. In order to best represent the real process, it is imperative to accurately estimate the probability distribution of input variables. MC simulation's output data is often displayed as probability distributions or transformed into error bars or confidence intervals. In this work, a MATLAB [68] script was written for performing MC simulation. Eq.(1) was used to compute the flow stress. Fig.2 shows the flowchart that was used to conduct the MC simulation. The MC simulation was run 10^6 times to have meaningful random variations.

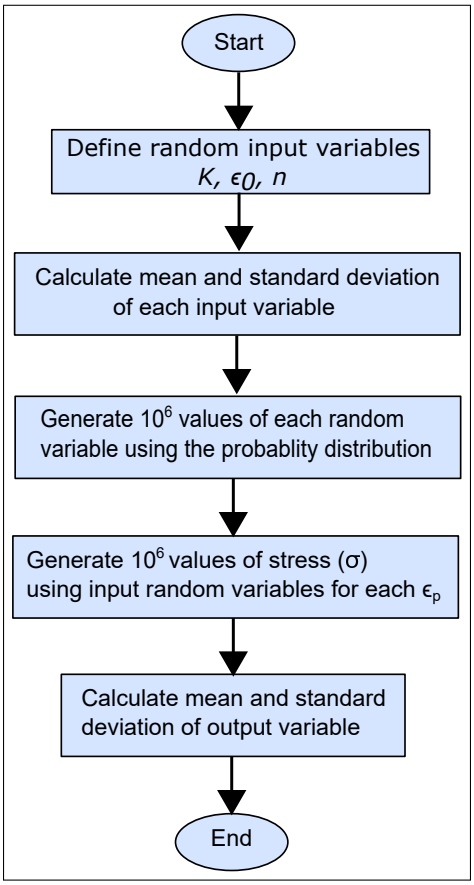

Fig. 2: Flow chart used for MC simulation.

To further validate the results obtained using a MATLAB program, the National Institute of Standards and Technology (NIST) uncertainty machine

was also used to compute the uncertainty. NIST uncertainty machine (Version 1.5) [69] is a freely available web-based software application based on a R script.

2.3 Sensitivity analysis

Sensitivity analysis aims to evaluate how the output quantity is affected by the variation in values of input parameters. The objective of sensitivity analysis is to understand the relative importance of an input parameter in the total output uncertainty. It helps to understand the most critical parameter that contributes to the uncertainty in the model output. In this work, sensitivity analysis of the Swift hardening law. was performed to determine the relative influence of different input parameters on the accuracy of flow stress estimation. The input material parameters of this model (Eq. (1)) are K, ϵ_0 and n. Sensitivity analysis was performed using a method of derivatives [70]. For example, the sensitivity of a given output function $Y = f(X1, X2, X3)$ for the input process variable X is defined as the partial derivative of Y with respect to $X1$ $\big($ i.e., $\partial Y/\partial X1\big)$. Sensitivity is often normalized by multiplying the standard deviations of the output and input parameters, as shown in Eq. (2) below [70]:

$$S_X^{\sigma} = \frac{\sigma_{X1}\partial Y}{\sigma_Y \partial X1} \tag{2}$$

where S_X^{σ} represents the sensitivity of output for an input variable X. Further, it is normalized by the standard deviations. σ_{X1} , σ_{X2} are the standard deviations of input and output quantity, respectively. Generally, the square of the sensitivity is reported because the summation of squares of sensitivity normalizes to 1 for N input variables. The square of sensitivity for n input variables is represented as shown below:

$$\sum_{i=1}^{N} \left(S_{X_i}^{\sigma}\right)^2 = 1 \tag{3}$$

A MATLAB script was written to perform the sensitivity analysis. Further, the results were also compared with those obtained from the NIST uncertainty machine.

3 Materials and methods

In the present work, DP600 steel of sheet thickness 2.6 mm and nominal chemical composition as mentioned earlier in Section 2.1 was chosen.

3.1 Hole expansion test

To evaluate the stretch-flangeability of the sheet metal, HET was conducted as per the ISO 16630 2009 standard. Figs. 3a and 3b show a schematic diagram of the HET deformation process. HET was conducted using a square blank of dimension 90×90 mm^2, with a central hole of 10 mm diameter. The HET

specimens' center hole was prepared using drilling and boring processes. A blank holding force of 65 kN was applied to hold the blank and prevent the draw-in of the sheet. A conical punch with a cone angle of 60° was used to deform the blank with a constant punch velocity of 10 mm/min. A video camera with a light source was used to record and monitor the experiment. The test was interrupted immediately upon the visual detection of a through-thickness crack. The output of the test is a non-dimensional ratio known as hole expansion ratio (HER), commonly expressed in terms of (%), which is calculated using Eq.(4).

$$HER(\%) = \frac{d_f - d_0}{d_0} \times 100 \tag{4}$$

where d_f and d_0 refer to the final and initial diameter of the central hole. d_f and d_0 are calculated using the average values of diameters measured at angles of 45°. All the experiments were repeated three times and average values along with standard deviation are reported.

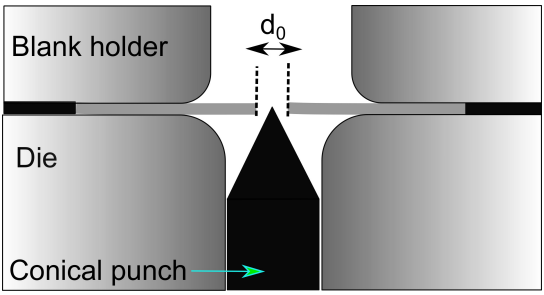

(a) Before HET

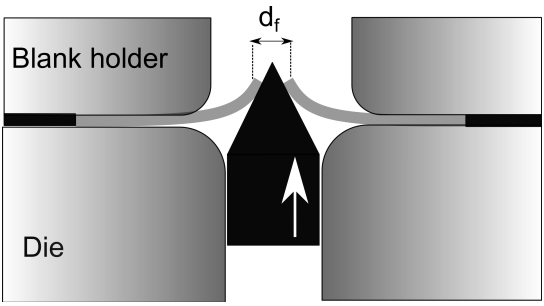

(b) After HET

Fig. 3: A schematic diagram of the HET deformation process (a) before the test, and (b) after test completion

3.2 Finite element simulation

To understand the effect of uncertainty in material parameters of the Swift hardening law in sheet metal stamping operations, Finite element (FE) analysis of hole expansion tests (HET) were performed. FE simulation was carried out using commercially available ABAQUS \Explicit 6.14 software [71]. A square blank of dimension 90×90 mm^2, with a central hole of diameter 10 mm and sheet thickness 2.6 mm, was modelled as a deformable body whereas a conical punch with a cone angle of 60° that was used for deforming the blank was modelled as analytically rigid. The conical punch was constrained to move only in the vertical direction with a constant punch velocity of 10 mm/min (Fig.4a). The blank was discretized using three-dimensional 8-node linear brick, reduced integration continuum elements (C3D8R). In the through-thickness direction, the blank was meshed with at least 10 elements, considering the large localized bending deformation. The mesh was chosen based on the mesh sensitivity study. Fig.5 shows the convergence study for the results of PEEQ in the hole expansion test. Near the hole region finer mesh were given, the total number of elements in the blank were approximately 61,180. The details of the mesh used in this simulation work is summarized in Table 3. A Coulomb friction model with a constant friction coefficient of 0.2 [32] was used to model the contact between the punch and the blank. Table 1 indicates that the material is not purely isotropic. However, due to limitations on the data availability in open literature, anisotropy is not included in the analysis. The deviation is, however, expected to be negligible. Given the closeness of the Lankford coefficients to unity isotropic hardening with von-Mises yield criteria was used to simulate the deformation behavior. The material response of the blank was modelled using the Swift hardening law, as in Eq.(1).

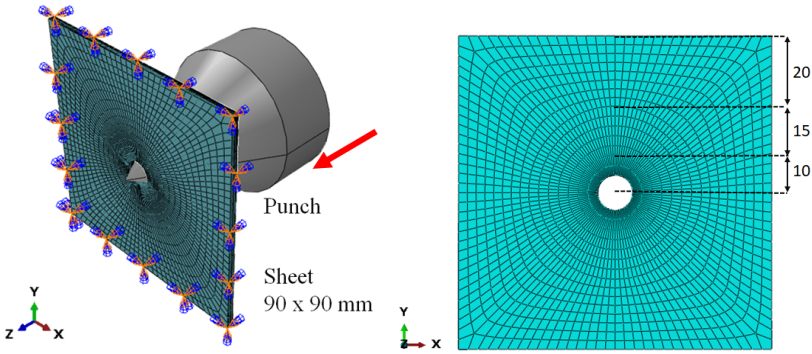

(a) Boundary condition (b) Mesh

Fig. 4: (a) Image showing Hole expansion test set up with boundary conditions (arrow indicates loading direction) (b) Image showing undeformed mesh configuration (numerical values indicate size of computational domain in mm).

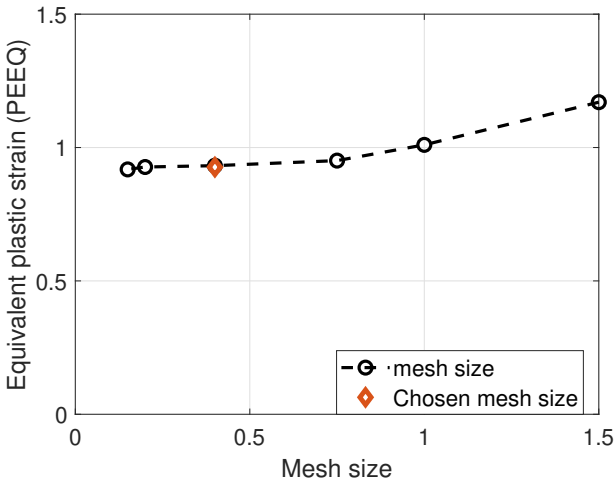

Fig. 5: Variation of PEEQ at with varying mesh sizes at the inner hole edge for $\mu + 2\sigma$ limits.

Table 3: Details of the meshing strategy used in the FE simulation.

Mesh Type	C3D8R
Mesh size, Inner region	0.4 mm
Mesh size, Middle region	1 mm
Mesh size, Outer edge	2.5 mm
Number of through thickness elements	10
Number of elements	61,180

Figs.6a and 6b shows the mean simulated stress-strain curve along with upper and lower limits for $(\mu \pm \sigma)$ and $(\mu \pm 2\sigma)$ limits that were used to define the input strain hardening behavior in the FE model to simulate the HET.

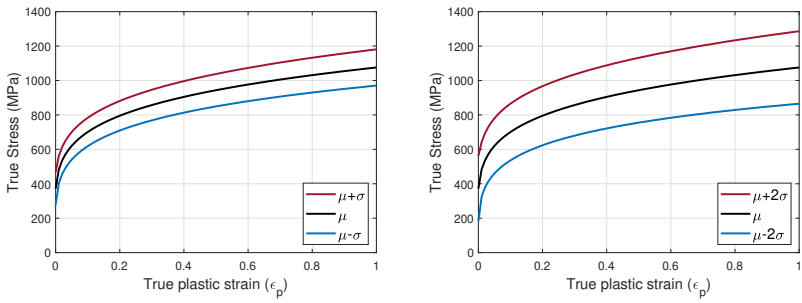

(a) Variation at $\mu \pm \sigma$ (b) Variation at $\mu \pm 2\sigma$

Fig. 6: True tensile stress–strain curves for (a) $(\mu \pm \sigma)$, (b) $(\mu \pm 2\sigma)$ as determined by the MC simulation for the Swift hardening law.

One of the critical aspects in HET is to estimate equivalent fracture strains (ϵ_{eq}). For this, equivalent fracture strains were estimated using Eq.(5) [72] by measuring the inner (d_{inner}) and outer (d_{outer}) hole diameter and sheet thickness (t_{edge}) around the circumference at fracture as shown below:

$$\epsilon_{eq} = \frac{2}{3}(\epsilon_c - \epsilon_t) \tag{5}$$

where ϵ_c and ϵ_t are the circumferential and thickness strain, respectively and are given by the following expressions:

$$\epsilon_c = \ln\left(\frac{d_{outer} + d_{inner}}{2d_o}\right) \tag{6}$$

$$\epsilon_t = \ln\left(\frac{t_{edge}}{t_o}\right) \tag{7}$$

where d_o and t_o are initial hole diameter and sheet thickness, respectively. For estimating the equivalent fracture strain from FE simulation in different edge conditions, the strain components (ϵ_c and ϵ_t) are estimated at

corresponding measured punch displacements at fracture. Since the punch displacements at fracture are sensitive to hole edge conditions, they are measured experimentally for each edge condition (drilling and boring).

4 Results and discussion

The microstructure of the selected steel is characterized. The details of the characterization procedure and results can be refereed in the Appendix A and B.

4.1 MC simulation

Fig. 7 shows the variation in the flow stress using the material parameters mentioned in Table 2 obtained with the Swift hardening law (Eq.(1)). Table 2 shows that there is a significant variation in the Swift hardening parameters for the DP600 steel. As explained earlier, these variations in the hardening parameters can be possibly attributed to various factors like scatter in material properties, variations in the chemical composition of the alloy, measurement errors, etc. The first and primary requirement for performing the stochastic analysis using MC simulation is to accurately estimate the probability distribution of input quantities that describes the actual process.

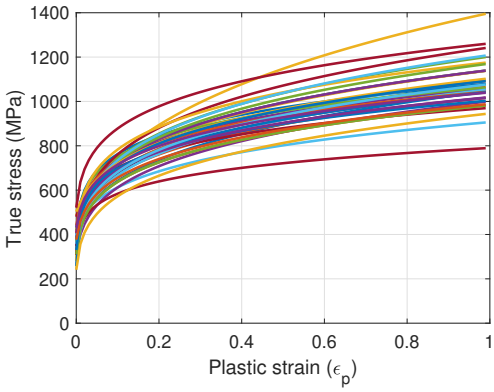

Fig. 7: Tensile stress-strain curves due to variations in Swift hardening law parameters.

In this work, the input parameters are K, ϵ_0, and n. Table 2 lists the values of these Swift hardening law parameters as reported by researchers. Based on these values, the probability distributions of these input parameters were identified using the MATLAB distribution fitter tool [73]. The probability distributions of these input parameters are shown in Fig. 8. It is observed that the parameter K follows an approximately normal distribution, while parameters ϵ_0 and n follow an approximately lognormal distribution.

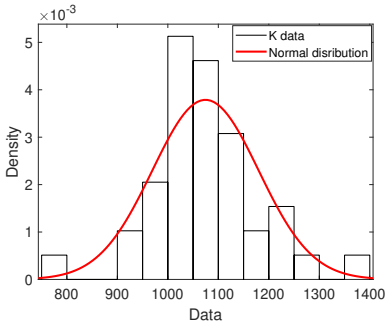

(a) Parameter K

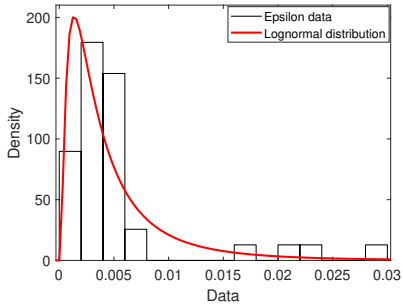

(b) Parameter ϵ_0

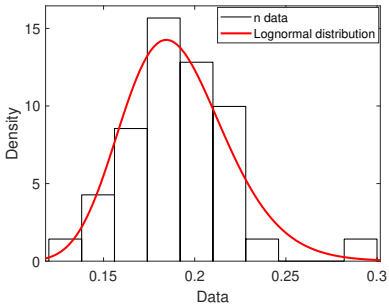

(c) Parameter n

Fig. 8: Probability density distribution of the various Swift hardening law parameters (a) parameter K - Normal distribution, (b) parameter ϵ_0 - Log normal distribution and (c) parameter n - Log normal distribution.

Further, various statistical parameters like mean (μ), standard deviation (σ), variance and coefficient of variation ($\frac{\sigma}{\mu}$) for these input parameters (K, ϵ_0 and n) were estimated and are tabulated in the Table 4.

Table 4: Statistical measure of input parameters for the Swift hardening law.

Input parameter	Mean	Standard deviation	Variance	Coefficient of variation	Distribution
K (MPa)	1075.02	103.99	10813.92	0.096	Normal
ϵ_0	0.0051	0.0062	0.000038	1.215	Lognormal
n	0.1906	0.0290	0.00841	0.152	Lognormal

After identifying the probability distribution of input parameters, uncertainties in stress computation at different plastic strains using the Swift hardening law were obtained by estimating the standard deviation. The computed uncertainty in the stress were obtained by MC simulations, in which 10^6 random samples were used to estimate the flow stress using the constitutive Eq. (1). The mean and standard deviation were computed at each true plastic strain. The computed flow curves based on the Swift law is shown in Fig.9. The $(\mu \pm \sigma)$ and $(\mu \pm 2\sigma)$ limits, representing 68% and 95% confidence intervals, are also shown in Figs.9 (a) and 9 (b) respectively.

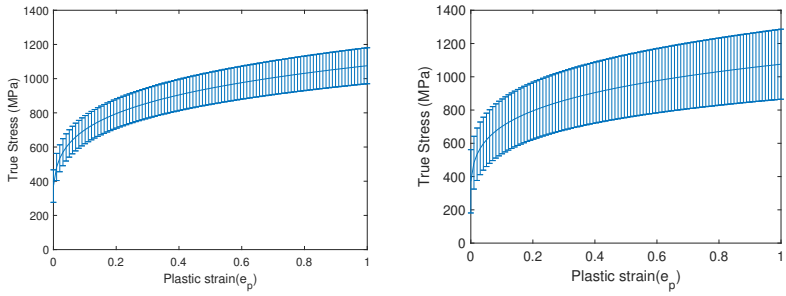

Fig. 9: Stochastic flow curves are generated using MC simulation for (a) $\mu \pm \sigma$ limit and (b) $\mu \pm 2\sigma$ limit.

Figs.9 (a) and 9 (b) show the stochastic stress-strain curve (mean stress-strain curve along with uncertainty). It is observed that the width of variation continuously increases with plastic strain in both cases. At plastic strain, $\epsilon_p = 1$, the $\pm\sigma$ limits and $\pm 2\sigma$ limits account for 9.78 % and 19.57 % of the mean.

4.2 Sensitivity analysis

As explained earlier in Section 2.3, sensitivity analysis aims to understand the most critical input variable that affects the uncertainty in the output function. The probability density functions mentioned in Table 4 are used to determine the sensitivity coefficients of the input variables. Based on the distribution function, the output function is calculated using Eq. (1). Sensitivity analysis was conducted using the method of derivatives explained in Section 2.3. Eq. (2)

was used to compute the sensitivities. Fig.10 shows the evolution of sensitivity coefficients with plastic strain. It is observed that the sensitivity coefficient for parameter K and n increases with plastic strain, while those for the other parameter (ϵ_0) decrease with the increase in plastic strain. The MATLAB results were compared with those from the NIST uncertainty machine. A very good agreement can be seen in these plots.

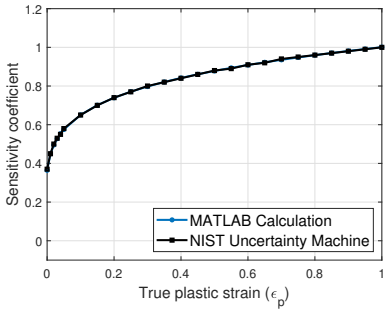

(a) Parameter K

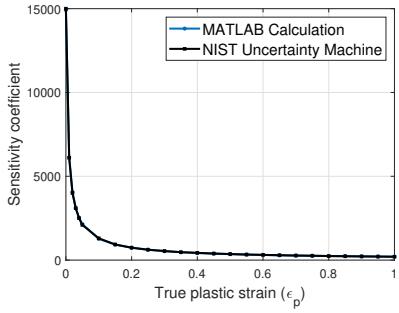

(b) Parameter ϵ_0

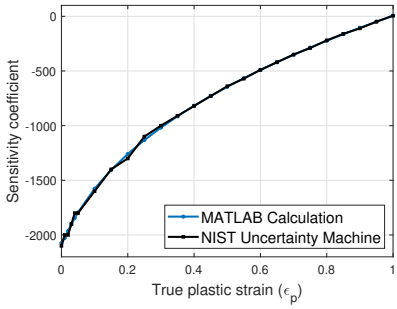

(c) Parameter n

Fig. 10: Evolution of sensitivity coefficients of the Swift hardening law parameters with true plastic strain (a) K, (b) ϵ_0, and (c) n.

The evolution of the normalized sensitivity coefficient (Eq.(2)) with true plastic strain, ϵ_p is shown in Fig. 11. On normalizing the sensitivities of the input parameters of the Swift hardening law (Eq.(1)) all sensitivity values lie within (0 to 1). This helps to effectively visualize and compare the estimated results. It is interesting to note that at $\epsilon_p = 0$, (i.e., stress corresponding to yield stress of the material), ϵ_0 is the most sensitive parameter. Whereas, as the material strain hardens with increasing plastic strain, the sensitivity for the parameter K monotonically increases and saturates to 1 and the sensitivity for the parameter n gradually decreases.

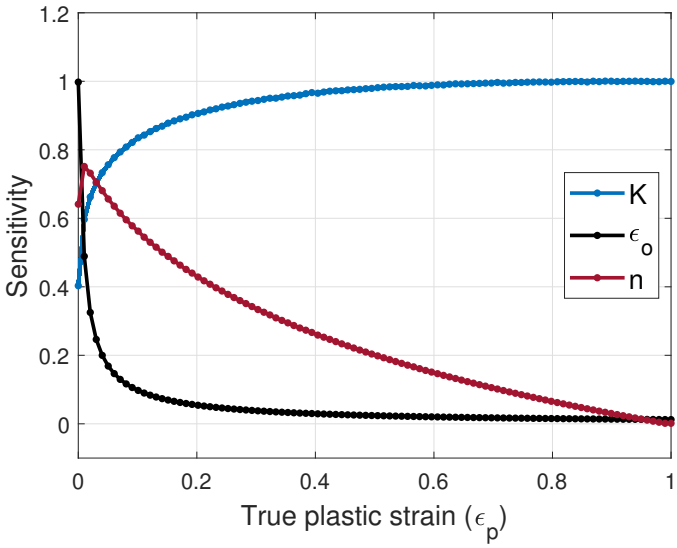

Fig. 11: Evolution of square of sensitivity coefficients of the various Swift hardening parameters with true plastic strain.

To elucidate the contributions of input parameters of the Swift hardening law (i.e., K, ϵ_0 and n) on the flow stress, the contribution of each of the individual parameters at different plastic strain increments is estimated using the NIST uncertainty machine. Analysis of variance (ANOVA) for the input material parameters at different plastic strains were estimated and tabulated in Table 5. It can be seen from Table 5 that at relatively lower plastic strains, parameters ϵ_0 and n contribute equally to the flow stress whereas, as the plastic strain increases there is a sudden decline in the percentage contribution from the parameter ϵ_0 while there is a gradual decrease in the percentage contribution from the parameter n. On the contrary, the contribution from the parameter K was found to monotonically increase and thereafter it tends to attain a saturated value. From this study, it is inferred that overall at large plastic strain the order of relative importance of material parameter is $K > n > \epsilon_0$, whereas, near the yield point where the material enters the plastic deformation regime the order of relative importance of material parameter is $\epsilon_0 > n > K$ (see Fig.11).

Table 5: ANOVA % contributions from input material parameters of the Swift hardening law (K, ϵ_0 and n) on the flow stress estimated using the NIST uncertainty machine.

Plastic strain (ϵ_p)	K (MPa)	ϵ_0	n
0.00	16.49	41.06	42.45
0.05	56.74	2.02	41.24
0.10	68.80	0.76	30.44
0.15	76.36	0.41	23.23
0.20	81.71	0.26	18.03
0.25	85.72	0.18	14.10
0.30	88.81	0.13	11.06
0.35	91.24	0.10	8.66
0.40	93.17	0.08	6.75
0.45	94.71	0.07	5.22
0.50	95.97	0.05	3.98
0.55	96.96	0.05	2.99
0.60	97.76	0.04	2.20
0.65	98.40	0.03	1.57
0.70	98.89	0.03	1.08
0.75	99.27	0.03	0.70
0.80	99.56	0.02	0.42
0.85	99.76	0.02	0.22
0.90	99.89	0.02	0.09
0.95	99.96	0.02	0.02
1.00	99.99	0.01	0.00

Such an analysis can be used as a guiding tool while obtaining the material parameters from experimental data. This will overall improve the accuracy of the numerical fitting and more robust hardening parameters can be extracted. Without having the knowledge of the most significant parameters, errors can unknowingly be introduced, which could adversely affect the accurate estimation of the output flow stresses.

4.3 Hole expansion test

The HET were conducted as mentioned earlier in Section 3.1. A typical HET specimen before and after the test is shown in Fig. (12a and 12b), respectively. The values of HER were estimated using Eq. (4). The experimentally determined HER values for drilled and bored edges are mentioned in Table 6. It is observed that the bored edge exhibited (7%) higher HER values compared to the drilled edge. It is widely accepted that the HER values are very much sensitive to the hole edge preparation method [28–30]. Typically, micro-cracks are generated during the center hole preparation. These micro-cracks serve as crack initiation sites during HET deformation. Since boring is a semi-finishing process, therefore the surface roughness values and micro-crack density are comparatively less than that of drilled edge. This observation is clearly supported, by the higher values of HER in the bored edge compared to the drilled edge.

Table 6: Comparison of HER (%) in different edge conditions.

Edge condition	HER (%)	Avg. surface roughness,Ra (μm)
Drilled edge	68 ± 14.3	4.32 ± 0.19
Bored edge	73.12 ± 8.66	2.32 ± 0.14

In a typical hole expansion test, the sheet metal continues to thin due to the force exerted by the punch. As the sheet metal continues to thin down, a through-thickness crack develops.

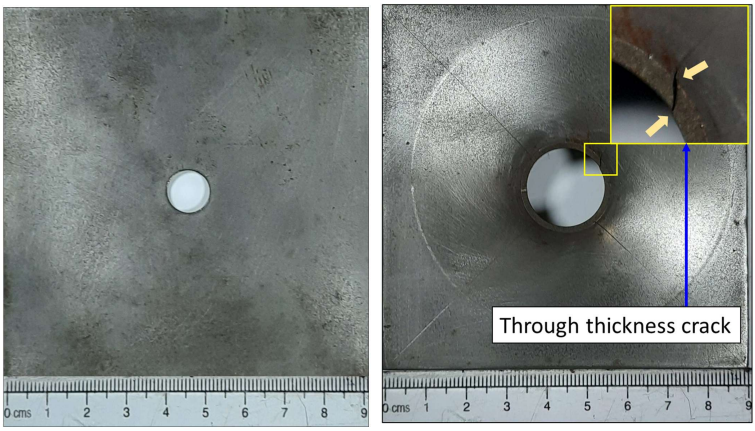

(a) Initial specimen (b) Deformed specimen

Fig. 12: HET specimen (a) Undeformed specimen, and (b) Deformed specimen after hole expansion test (Bored edge).

The reduction in sheet thickness at the hole edge with punch displacement was estimated for the mean (μ) and ($\mu \pm \sigma$) and ($\mu \pm 2\sigma$) limits. The results are shown in Fig.13. It was observed that the predicted thickness reduction using the mean (μ) input material data was always lying in the center of the two predicted thickness reduction curves using ($\pm\sigma$, $\pm$ 2σ) limits. Higher reduction in sheet thickness was observed for ($\mu - \sigma$, $\mu - 2\sigma$) compared to ($\mu + \sigma$, $\mu + 2\sigma$) limits. These statistical limits represent the variation in the strength of the material, and it is known that in a ductile metallic material higher strength leads to greater resistance towards through thickness deformation. Therefore, the resistance to thinning will be higher in case of ($\mu + \sigma$, $\mu + 2\sigma$) compared to that for ($\mu - \sigma$, $\mu - 2\sigma$). To further validate this prediction, the sheet thickness of the deformed specimen (Fig.12(b).) for different edge conditions (drilled edge, bored edge) at the fracture was experimentally measured,

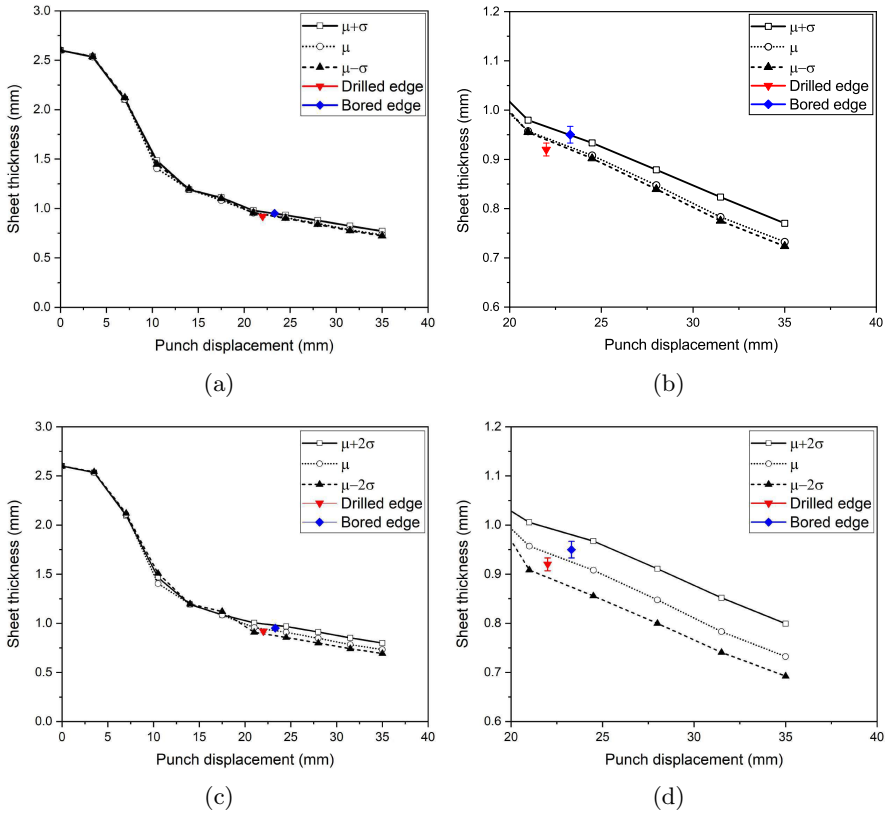

Fig. 13: Variation of sheet thickness along with the punch displacement (a) simulated using ($\mu \pm \sigma$), (b) enlarged view of sub-figure (a), (c) simulated using ($\mu \pm 2\sigma$), and (d) enlarged view of sub-figure (c).

and it is superposed in the simulated curves (see Fig.13). It is observed that the experimental values are well within the predicted limits. It is interesting to note that irrespective of input material limits, the rate of sheet thickness reduction (Δt) is high in the initial deformation regime but as the punch continues to deform the blank the rate of sheet thickness reduction decreases. This is because initially the conical punch is in contact with the sheet, and it exerts the compressive stress in the radial direction, but as the deformation continues the inner edge of the sheet is no longer in contact with the punch. A similar observation of punch detachment with the sheet was experimentally demonstrated by [74]. Another interesting observation can be made from Fig.13. The experimental values of sheet thickness for both bored and drilled edge conditions are contained within ($\mu \pm 2\sigma$) plots (see Fig.13c and Fig.13d.) Therefore, simulations containing ($\pm 2\sigma$) bounds of mean flow stresses are likely to provide more accurate estimations of the actual material behavior during forming operations.

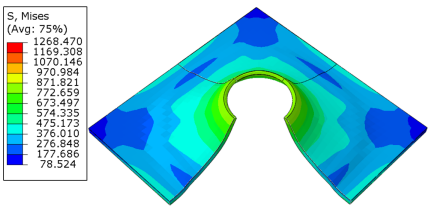

(a) S.Mises distribution for $\mu - 2\sigma$ limit

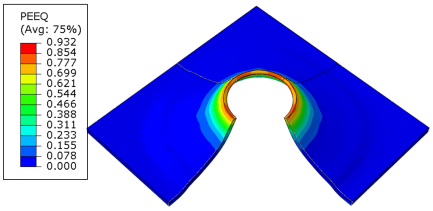

(b) PEEQ distribution for $\mu - 2\sigma$ limit

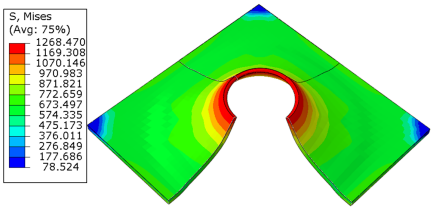

(c) S.Mises distribution for $\mu + 2\sigma$ limit

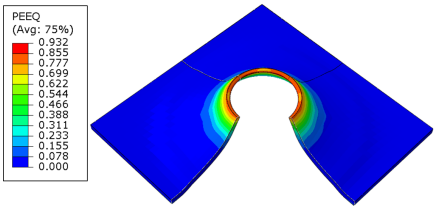

(d) PEEQ distribution for $\mu + 2\sigma$ limit

Fig. 14: FE simulation of hole expansion test distribution of (a) von Mises equivalent stress, (b) equivalent plastic strain for $(\mu - 2\sigma)$ limit, (c) von Mises equivalent stress and (d) equivalent plastic strain for $(\mu + 2\sigma)$ limit at 35 mm punch displacement.

To further understand the effect of variation in mechanical properties, the distribution of von Mises stress and equivalent plastic strain (PEEQ) for the $(\mu - 2\sigma,\ \mu + 2\sigma)$ limits were compared at a punch displacement of 35 mm as shown in Fig.14. It is observed that deformation is predominately concentrated at the hole edge. However, for the same punch displacement, there is significant variation in the von Mises stress distribution for $(\mu - 2\sigma)$ compared to $(\mu + 2\sigma)$ limit. Note that the punch displacement can be indirectly correlated with the equivalent plastic strain (PEEQ) imposed during HET. It is observed from Fig.14b and Fig.14d that the PEEQ distribution is nearly the same in both cases however, there is significant variation in the von Mises stress distribution in the HET specimen. The $(\mu - 2\sigma)$ limit corresponds to much softer material behavior compared to that for the $(\mu + 2\sigma)$ limit. Therefore, for achieving the same equivalent plastic strain (PEEQ) a harder material needs a larger deforming force, thereby developing larger von Mises stress in the specimen [75] which also supports our earlier observation of a large reduction in the sheet thickness.

It is well established that the edge condition plays a crucial role in hole expansion tests due to the existence of pre-existing defects that are generated during manufacturing. The sheet fracture takes place at larger punch travel and thus larger reduction takes place. The accurate simulation will lead to a better estimation of hole expansion ratio (HER), which is a major challenge in the automotive sector. To further understand the influence of the edge

condition, an additional statistical description is provided. For this purpose, the maximum, minimum, and median values associated with the strain measurement are estimated at experimentally determined punch displacement at fracture as explained in Section 3.2. A box and whisker plot pertaining to strain measurement in different edge conditions is shown in Fig.15. It is seen that the measured strain in the bored edge is higher than the drilled edge. Larger variability for the bored edge condition is shown, which is expected because of the higher propensity for defect formation during manufacturing operation for this process. Higher median values in comparison to mean values for both edge conditions indicate that, statistically, there are higher number of larger equivalent strain values at fracture than those with lower fracture strains.

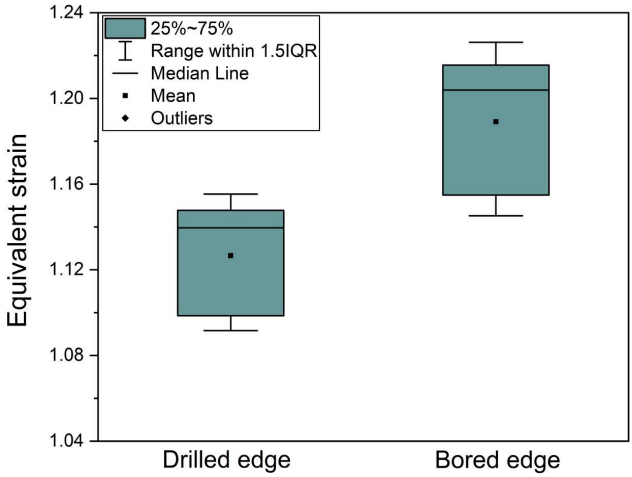

Fig. 15: Box and Whisker plot of equivalent strain in different edge condition estimated using FE simulation.

5 Conclusions

A MC-based approach was used to obtain the uncertainty in the true stress estimation based on the Swift hardening law using uniaxial stress-strain data reported in the literature and those from three tests conducted in this study. A sensitivity analysis was performed to understand the most critical parameters of the Swift hardening law, affecting the uncertainties in estimated flow stresses. Thereafter, the obtained mean and standard deviations for the true stress-strain curves for ($\mu \pm \sigma$) and ($\mu \pm 2\sigma$) limits were used to simulate the hole expansion test (HET) using FE simulation. Following important conclusions can be made from the present study.

1. Sensitivity coefficients of the Swift hardening parameters are dependent on the true plastic strain. At lower plastic strains ϵ_0 was found to be most sensitive parameter whereas at larger pre-strains K was observed to be the critical parameter affecting the flow stress estimation.
2. The reduction in sheet thickness was sensitive to the uncertainty limits. It is shown that the larger reduction in sheet happens for $(\mu - 2\sigma)$ limit compared to that for $(\mu + 2\sigma)$ limit.
3. The experimental values lie within the statistical limits determined from FE simulations using the bounds of the Swift hardening law as determined from the MC simulations, and a close match was observed.
4. The present study demonstrates that uncertainties of parameters of more complicated hardening laws and their relative influences on the hardening behavior of the material can be determined by pursuing a similar approach.

6 Acknowledgement

The authors would like to acknowledge ArcelorMittal for supplying the steel used in this work. One of the author, Kali Prasad acknowledges Dr. Rahul Kumar, Research Scholar, Department of Applied Mechanics, IIT Madras for fruitful discussions.

A Initial material characterization

For the metallographic examination, standard metallographic procedures were used to polish the as received sample and then etched with 2% nital reagent for 10-12 s. The microstructure was observed using a scanning electron microscope (SEM) (Inspect F50 from FEI).

B Material characterization results

he microstructure of the as-received steel sheet is shown in Fig.16. Microstructure reveals the presence of uniformly distributed martensite phase in the ferrite matrix, with a phase fraction of martensite as 22 ± 1%. The average

grain size of ferrite and martensite phase is approximately 4.1 ± 1.6 μm, 2.5 ± 1.4 μm, respectively.

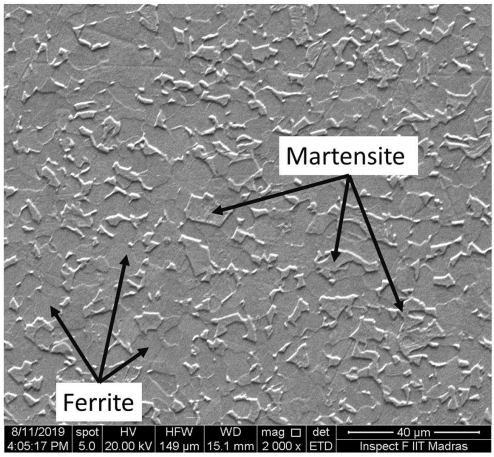

Fig. 16: Microstructure of as received DP600 steel.

References

[1] Kim, J.-H., Serpantié, A., Barlat, F., Pierron, F., Lee, M.-G.: Characterization of the post-necking strain hardening behavior using the virtual fields method. International Journal of Solids and Structures **50**(24), 3829–3842 (2013). https://doi.org/10.1016/j.ijsolstr.2013.07.018

[2] Enami, K.: The effects of compressive and tensile prestrain on ductile fracture initiation in steels. Engineering Fracture Mechanics **72**(7), 1089–1105 (2005). https://doi.org/10.1016/j.engfracmech.2004.07.012

[3] Iadicola, M.A.: Uncertainties of digital image correlation due to pattern degradation at large strain. In: Jin, H., Yoshida, S., Lamberti, L., Lin, M.-T. (eds.) Advancement of Optical Methods in Experimental Mechanics, Volume 3, pp. 247–253. Springer, Cham (2016)

[4] Badadani, V., Sriranga, T.S., Srivatsa, S.R.: Analysis of uncertainty in digital image correlation technique for strain measurement. Materials Today: Proceedings **5**(10, Part 1), 20912–20919 (2018). https://doi.org/10.1016/j.matpr.2018.06.479. International Conference on Smart Engineering Materials (ICSEM 2016), October 20-22, 2016

[5] Siebert, T., Hack, E., G.Lampeas, Patterson, E.A., K.Splitthof: Uncertainty quantification for dic displacement measurements in industrial environments. Experimental Techniques **45**, 685–694 (2021). https://doi.org/10.1007/s40799-021-00447-3

[6] Berbenni, S., Favier, V., Berveiller, M.: Impact of the grain size distribution on the yield stress of heterogeneous materials. International Journal of Plasticity **23**(1), 114–142 (2007). https://doi.org/10.1016/j.ijplas.2006.03.004

[7] Weiss, M., Abeyrathna, B., Rolfe, B., Abee, A., Wolfkamp, H.: Effect of coil set on shape defects in roll forming steel strip. Journal of Manufacturing Processes **25**, 8–15 (2017). https://doi.org/10.1016/j.jmapro.2016.10.005

[8] Aggogeri, F., Barbato, G., Barini, E.M., Genta, G., Levi, R.: Measurement uncertainty assessment of coordinate measuring machines by simulation and planned experimentation. CIRP Journal of Manufacturing Science and Technology **4**(1), 51–56 (2011). https://doi.org/10.1016/j.cirpj.2011.01.007. Special Section on Innovative and Cognitive Manufacturing Engineering

[9] Banerjee, D.K.: Uncertainties in steel temperatures during fire. Fire Safety Journal **61**, 65–71 (2013). https://doi.org/10.1016/j.firesaf.2013.08.012

[10] Lazarescu, L., Banabic, D.: Influence of material property variability on the thickness in sheet metal subjected to the hydraulic bulging. In: Interdisciplinary Research in Engineering: Steps Towards Breakthrough Innovation for Sustainable Development. Advanced Engineering Forum, vol. 8, pp. 251–258. Trans Tech Publications Ltd, ??? (2013). https://doi.org/10.4028/www.scientific.net/AEF.8-9.251

[11] Janssens, K., Lambert, F., Vanrostenberghe, S., Vermeulen, M.: Statistical evaluation of the uncertainty of experimentally characterised forming limits of sheet steel. Journal of Materials Processing Technology **112**(2), 174–184 (2001). https://doi.org/10.1016/S0924-0136(00)00890-6

[12] Banabic, D., Vos, M.: Modelling of the forming limit band –a new method to increase the robustness in the simulation of sheet metal forming processes. CIRP Annals **56**(1), 249–252 (2007). https://doi.org/10.1016/j.cirp.2007.05.058

[13] El Khoukhi, D., Morel, F., Saintier, N., Bellett, D., Osmond, P., Le, V.-D.: Probabilistic modeling of the size effect and scatter in high cycle fatigue using a monte-carlo approach: Role of the defect population in cast aluminum alloys. International Journal of Fatigue **147**, 106177 (2021). https://doi.org/10.1016/j.ijfatigue.2021.106177

[14] Geiger, M., Merklein, M.: Determination of forming limit diagrams – a new analysis method for characterization of materials' formability. CIRP Annals **52**(1), 213–216 (2003). https://doi.org/10.1016/S0007-8506(07)60568-X

[15] De Souza, T., Rolfe, B.F.: Characterising material and process variation effects on springback robustness for a semi-cylindrical sheet metal forming process. International Journal of Mechanical Sciences **52**(12), 1756–1766 (2010). https://doi.org/10.1016/j.ijmecsci.2010.09.009

[16] De Souza, T., Rolfe, B.: Multivariate modelling of variability in sheet metal forming. Journal of Materials Processing Technology **203**(1), 1–12 (2008). https://doi.org/10.1016/j.jmatprotec.2007.09.075

[17] Karthik, V., Comstock, R.J., Hershberger, D.L., Wagoner, R.H.: Variability of sheet formability and formability testing. Journal of Materials Processing Technology **121**(2), 350–362 (2002). https://doi.org/10.1016/S0924-0136(01)01219-5

[18] Basak, S., Panda, S.K.: Necking and fracture limit analyses of different pre-strained sheet materials in polar effective plastic strain locus using yld2000-2d yield model. Journal of Materials Processing Technology **267**, 289–307 (2019). https://doi.org/10.1016/j.jmatprotec.2018.10.004

[19] Graf, A., Hosford, W.: The influence of strain-path changes on forming limit diagrams of a1 6111 t4. International Journal of Mechanical Sciences **36**(10), 897–910 (1994). https://doi.org/10.1016/0020-7403(94)90053-1

[20] Huang, Y.-M., Cheng, J.-W.: Influence of lubricant on limitation of formability of cylindrical cup-drawing. Journal of Materials Processing Technology **63**(1), 77–82 (1997). https://doi.org/10.1016/S0924-0136(96)02603-9

[21] Prasad, K., Gupta, A., Krishnaswamy, U.C., Banerjee, D.K., Lee, M.-G.: Does friction contribute to formability improvement using servo press ? Friction (2022)

[22] Narayanasamy, R., Narayanan, C.S.: Experimental analysis and evaluation of forming limit diagram for interstitial free steels. Materials Design **28**(5), 1490–1512 (2007). https://doi.org/10.1016/j.matdes.2006.03.010

[23] Narasimhan, K., Zhou, D., Wagoner, R.H.: Application of the monte carlo and finite element methods to predict the scatter band in forming limit strains. Scripta Metallurgica Et Materialia **26**, 41–46 (1992)

[24] Durrenberger, L., Lemoine, X., Molinari, A.: Effects of pre-strain and bake-hardening on the crash properties of a top-hat section. Journal of Materials Processing Technology **211**(12), 1937–1947 (2011). https://doi.org/10.1016/j.jmatprotec.2011.06.015

[25] Bekar, D., Acar, E., Ozer, F., Guler, M.: Robust springback optimization of a dual phase steel seven-flange die assembly. Structural and Multidisciplinary Optimization **46**, 425–444 (2012). https://doi.org/10.1007/s00158-012-0771-y

[26] Mohr, D., Dunand, M., Kim, K.-H.: Evaluation of associated and non-associated quadratic plasticity models for advanced high strength steel sheets under multi-axial loading. International Journal of Plasticity **26**(7), 939–956 (2010). https://doi.org/10.1016/j.ijplas.2009.11.006

[27] Padmanabhan, R., Baptista, A.J., Oliveira, M.C., Menezes, L.F.: Effect of anisotropy on the deep-drawing of mild steel and dual-phase steel tailor-welded blanks. Journal of Materials Processing Technology **184**(1), 288–293 (2007). https://doi.org/10.1016/j.jmatprotec.2006.11.051

[28] Paul, S.K., Mukherjee, M., Kundu, S., Chandra, S.: Prediction of hole expansion ratio for automotive grade steels. Computational Materials Science **89**, 189–197 (2014). https://doi.org/10.1016/j.commatsci.2014.03.040

[29] Prasad, K., Venkatesh, B., Krishnaswamy, H., Banerjee, D.K., Chakkingal, U.: On the interplay of friction and stress relaxation to improve stretch-flangeability of dual phase (DP600) steel. CIRP Journal of Manufacturing Science and Technology **32**, 154–169 (2021). https://doi.org/10.1016/j.cirpj.2020.11.014

[30] Paul, S.K.: A critical review on hole expansion ratio. Materialia **9**, 100566 (2020). https://doi.org/10.1016/j.mtla.2019.100566

[31] Prasad, K., Ebrahim, A.S., Krishnaswamy, H., Chakkingal, U., Banerjee, D.K.: Evaluation of hole expansion formability of high strength AA7075 alloy under varying temper conditions. IOP Conference Series: Materials Science and Engineering **1238**(1), 012038 (2022). https://doi.org/10.1088/1757-899x/1238/1/012038

[32] Prasad, K., Krisnaswamy, H., Banerjee, D., Chakkingal, U.: An investigation into the influence of interrupted loading in improving the stretch-flangeability of dual phase steel. In: Tribology in Manufacturing

Processes. Defect and Diffusion Forum, vol. 414, pp. 81–87. Trans Tech Publications Ltd, ??? (2022)

[33] ASTM E8 / E8M-16a, Standard test methods for tension testing of metallic materials,2016. Technical report, ASTM International, West Conshohocken, PA. https://doi.org/10.1520/E0008_E0008M-16A

[34] Chung, K.-H., Lee, W., Kim, J.H., Kim, C., Park, S.H., Kwon, D., Chung, K.: Characterization of mechanical properties by indentation tests and fe analysis – validation by application to a weld zone of DP590 steel. International Journal of Solids and Structures **46**(2), 344–363 (2009). https://doi.org/10.1016/j.ijsolstr.2008.08.041

[35] Reisgen, U., Schleser, M., Mokrov, O., Ahmed, E.: Uni- and bi-axial deformation behavior of laser welded advanced high strength steel sheets. Journal of Materials Processing Technology **210**(15), 2188–2196 (2010). https://doi.org/10.1016/j.jmatprotec.2010.08.003

[36] Suttner, S., Kuppert, A.: Investigation of the beginning of plastic yielding and the hardening behaviour under biaxial tension. In: WGP Congress 2013. Advanced Materials Research, vol. 769, pp. 197–204. Trans Tech Publications Ltd, ??? (2013). https://doi.org/10.4028/www.scientific.net/AMR.769.197

[37] Ahmed, E., Reisgen, U., Schleser, M., Mokrov, O.: Biaxial behavior of laser welded DP/TRIP steel sheets. The International Journal of Advanced Manufacturing Technology **339**, 1075–1082 (2013). https://doi.org/10.1007/s00170-013-4898-9

[38] Choi, K.Y., Lee, M.-G., Kim, H.-A.: Sheet metal forming simulation considering die deformation. International Journal of Automotive Technology **14**, 935–940 (2013)

[39] Taherizadeh, A., Green, D.E., Yoon, J.W.: A non-associated plasticity model with anisotropic and nonlinear kinematic hardening for simulation of sheet metal forming. International Journal of Solids and Structures **69-70**, 370–382 (2015). https://doi.org/10.1016/j.ijsolstr.2015.05.013

[40] Cardoso, M.C., Moreira, L.P.: Forming Limit Analysis of DP600-800 Steels. Zenodo (2015). https://doi.org/10.5281/zenodo.1108508

[41] Basak, S., Panda, S.K., Zhou, Y.N.: Formability Assessment of Prestrained Automotive Grade Steel Sheets Using Stress Based and Polar Effective Plastic Strain-Forming Limit Diagram. Journal of Engineering Materials and Technology **137**(4) (2015). https://doi.org/10.1115/1.4030786. 041006

[42] Basak, S., Panda, S.K.: Application of Barlat Yld-96 Yield Criterion for Predicting Formability of Pre-Strained Dual Phase Steel Sheets. International Manufacturing Science and Engineering Conference, vol. Volume 1: Processing (2016). https://doi.org/10.1115/MSEC2016-8753. V001T02A063

[43] Drotleff, K., Panich, S., Liewald, M., Uthaisangsuk, V.: Experimental and numerical formability analysis of advanced high strength steel for deep drawing using the nonlinear strain path forming limit. (2016)

[44] Basak, S., Panda, S.: Application of barlat yld-96 yield criterion for predicting formability of pre-strained dual phase steel sheets, pp. 001–02063 (2016). https://doi.org/10.1115/MSEC2016-8753

[45] Reis, L.C., Oliveira, M.C., Santos, A.D., Fernandes, J.V.: On the determination of the work hardening curve using the bulge test. International Journal of Mechanical Sciences **105**, 158–181 (2016). https://doi.org/10.1016/j.ijmecsci.2015.11.009

[46] Comsa, D.-S., Lazarescu, L., Banabic, D.: Assessing the formability of metallic sheets by means of localized and diffuse necking models, vol. 1769, p. 200010 (2016). https://doi.org/10.1063/1.4963628

[47] Isik, K., Gerstein, G., Gutknecht, F., Clausmeyer, T., Nürnberger, F., Maier, H.J., Tekkaya, A.E.: Investigations of ductile damage in DP600 and dc04 deep drawing steel sheets during punching. Procedia Structural Integrity **2**, 673–680 (2016). https://doi.org/10.1016/j.prostr.2016.06.087. 21st European Conference on Fracture, ECF21, 20-24 June 2016, Catania, Italy

[48] Bandyopadhyay, K., Lee, M.-G., Panda, S.K., Saha, P., Lee, J.: Formability assessment and failure prediction of laser welded dual phase steel blanks using anisotropic plastic properties. International Journal of Mechanical Sciences **126**, 203–221 (2017). https://doi.org/10.1016/j.ijmecsci.2017.03.022

[49] Qin, S., McLendon, R., Oancea, V., Beese, A.M.: Micromechanics of multiaxial plasticity of DP600: Experiments and microstructural deformation modeling. Materials Science and Engineering: A **721**, 168–178 (2018). https://doi.org/10.1016/j.msea.2018.02.078

[50] Szabolcs, J., Tisza, M.: Finite element modelling of clinched joints. Advanced Technologies Materials **43**, 1–6 (2018). https://doi.org/10.24867/ATM-2018-1-001

[51] Santos, R.O., da Silveira, L.B., Moreira, L.P., Cardoso, M.C., da Silva, F.R.F., dos Santos Paula, A., Albertacci, D.A.: Damage identification

parameters of dual-phase 600–800 steels based on experimental void analysis and finite element simulations. Journal of Materials Research and Technology **8**(1), 644–659 (2019). https://doi.org/10.1016/j.jmrt.2018.04.017

[52] Aksen, T.A., Sener, B., Firat, M.: Failure prediction capability of generalized plastic work criterion. Procedia Manufacturing **47**, 1235–1240 (2020). https://doi.org/10.1016/j.promfg.2020.04.190. 23rd International Conference on Material Forming

[53] Qin, S., Beese, A.M.: Multiaxial fracture of DP600: Experiments and finite element modeling. Materials Science and Engineering: A **785**, 139386 (2020). https://doi.org/10.1016/j.msea.2020.139386

[54] Béres, G., Lukács, Z., Tisza, M.: Springback evaluation of tailor welded blanks at v-die bending made of DP steels. Procedia Manufacturing **47**, 1366–1373 (2020). https://doi.org/10.1016/j.promfg.2020.04.266. 23rd International Conference on Material Forming

[55] Cheng, C., Wan, M., Wu, X.D., Cai, Z.Y., Zhao, R., Meng, B.: Effect of yield criteria on the formability prediction of dual-phase steel sheets. International Journal of Mechanical Sciences **133**, 28–41 (2017). https://doi.org/10.1016/j.ijmecsci.2017.08.033

[56] Bandyopadhyay, K., Basak, S., Panda, S.K., Saha, P.: Use of stress based forming limit diagram to predict formability in two-stage forming of tailor welded blanks. Materials Design **67**, 558–570 (2015). https://doi.org/10.1016/j.matdes.2014.10.089

[57] Neto, D.M., Oliveira, M.C., Santos, A.D., Alves, J.L., Menezes, L.F.: Influence of boundary conditions on the prediction of springback and wrinkling in sheet metal forming. International Journal of Mechanical Sciences **122**, 244–254 (2017). https://doi.org/10.1016/j.ijmecsci.2017.01.037

[58] Pandya, K.S., Grolleau, V., Roth, C.C., Mohr, D.: Fracture response of resistance spot welded dual phase steel sheets: Experiments and modeling. International Journal of Mechanical Sciences **187**, 105869 (2020). https://doi.org/10.1016/j.ijmecsci.2020.105869

[59] He, J., Cedric Xia, Z., Zeng, D., Li, S.: Forming Limits of a Sheet Metal After Continuous-Bending-Under-Tension Loading. Journal of Engineering Materials and Technology **135**(3) (2013). https://doi.org/10.1115/1.4023676. 031009

[60] Marcadet, S., Mohr, D.: Critical hardening rate model for predicting path-dependent ductile fracture. International Journal of Fracture **200**, 77–98 (2016). https://doi.org/10.1007/s10704-016-0130-x

[61] Shenghua, w., Song, N., Santos, A., Andrade Pires, F., Amaral, R.: Formability prediction for dual phase steel sheets, pp. 1–13 (2016)

[62] Gerstein, G., Isik, K., Gutknecht, F., Sieczkarek, P., Ewert, J., Tekkaya, A.E., Clausmeyer, T., Nürnberger, F.: Microstructural characterization and simulation of damage for geared sheet components. Journal of Physics: Conference Series **896**, 012076 (2017). https://doi.org/10.1088/1742-6596/896/1/012076

[63] Hashemi, R., Assempour, A., Abad, E.M.K.: Implementation of the forming limit stress diagram to obtain suitable load path in tube hydroforming considering m–k model. Materials Design **30**(9), 3545–3553 (2009). https://doi.org/10.1016/j.matdes.2009.03.002

[64] Bui-Van, A., Allain, S., Lemoine, X., Bouaziz, O.: An improved physically based behaviour law for ferritic steels and its application to crash modelling. International Journal of Material Forming **2**, 527–530 (2009). https://doi.org/10.1007/s12289-009-0539-0

[65] Pathak, C. N.and Butcher, Worswick, M.J.: Experimental techniques for finite shear strain measurement within two advanced high strength steels. Experimental Mechanics **59**, 125–148 (2019). https://doi.org/10.1007/s11340-018-00448-1

[66] Padmanabhan, R., Oliveira, M.C., Menezes, L.F.: Deep drawing of aluminium–steel tailor-welded blanks. Materials Design **29**(1), 154–160 (2008). https://doi.org/10.1016/j.matdes.2006.11.007

[67] Marques, A.E., Prates, P.A., Pereira, A.F.G., Oliveira, M.C., Fernandes, J.V., Ribeiro, B.M.: Performance comparison of parametric and non-parametric regression models for uncertainty analysis of sheet metal forming processes. Metals **10**(4) (2020). https://doi.org/10.3390/met10040457

[68] MATLAB: R2019b. The MathWorks, Inc. Natick, MA (2019)

[69] Lafarge, T., Possolo, A.: The NIST uncertainty machine. NCSLI Measure **10**(3), 20–27 (2015). https://doi.org/10.1080/19315775.2015.11721732

[70] Islam, F., Joannès, S., Laiarinandrasana, L.: Evaluation of critical parameters in tensile strength measurement of single fibres. Journal of Composites Science **3**(3) (2019). https://doi.org/10.3390/jcs3030069

[71] ABAQUS Documentation: Version 6.14. Dassault Systemes Simulia Corporation **651**(6.2) (2014)

[72] Butcher, C., Kortenaar, L.T., Worswick, M.: Experimental characterization of the sheared edge formability of boron steel, IDDRG,Paris, France (2014)

[73] MATLAB: Statistics Toolbox, Distribution Fitting Tool, R2019b (2019)

[74] Krempaszky, C., Larour, P., Freudenthaler, J., Werner, E.: Towards more efficient hole expansion testing, IDDRG,Paris, France (2014)

[75] Miranda, S., Cruz, D., Amaral, R., Santos, A., de Sá, J.C., Fernandes, J.: Assessment of scatter on material properties and its influence on formability in hole expansion. Proceedings of the Institution of Mechanical Engineers, Part L: Journal of Materials: Design and Applications **235**(6), 1262–1270 (2021)